Tribology Letters (2025) 73:134
https://doi.org/10.1007/s11249-025-02064-2

ORIGINAL PAPER

Sliding Friction of Hard Sliders on Rubber: Theory and Experiment

R. Xu[1,2,3,4] **· B. N. J. Persson**[1,2,3,4]

Received: 24 May 2025 / Accepted: 29 August 2025 / Published online: 17 September 2025

Abstract

We present a study of sliding friction for rigid triangular steel sliders on soft rubber substrates under both lubricated and dry conditions. For rubber surfaces lubricated with a thin film of silicone oil, the measured sliding friction at room temperature agrees well with theoretical predictions obtained from a viscoelastic model originally developed for rolling friction. On the lubricated surface, the sliding friction is primarily due to bulk viscoelastic energy dissipation in the rubber. The model, which includes strain-dependent softening of the rubber modulus, accurately predicts the experimental friction curves. At lower temperatures ($T = -20°C$ and $-40°C$), the measured friction exceeds the theoretical prediction. We attribute this increase to penetration of the lubricant film by surface asperities, leading to a larger adhesive contribution. For dry surfaces, the adhesive contribution becomes dominant. By subtracting the viscoelastic component inferred from the lubricated case, we estimate the interfacial frictional shear stress. This shear stress increases approximately linearly with the logarithm of the sliding speed, consistent with stress-augmented thermal activation mechanisms.

keywords Sliding friction · Viscoelasticity · Strain softening

1 Introduction

Rubber sliding friction plays a critical role in many applications, including tires, rubber seals, and damping systems. In such systems, frictional behavior is a result of the combined effects of viscoelastic energy dissipation and adhesion, which is influenced by a complex interplay between contact and environmental conditions such as surface roughness, lubrication, and temperature.

In this study, we investigate the sliding friction of rigid triangular steel sliders on soft rubber substrates under both dry and lubricated conditions. This problem has been studied previously by Greenwood and Tabor [1] (see also [2]), who demonstrated the importance of viscoelastic contributions to friction and discussed the role of lubricant film rupture and rubber damage for sharp contacts. However, a detailed quantitative comparison between experimental results and theoretical predictions for viscoelastic friction, including nonlinear strain effects, has been lacking.

Here, we present new experimental results and compare them with a theoretical model originally developed for rolling friction [3], which can be extended to sliding friction when the adhesive contribution is negligible. This is typically the case for lubricated interfaces where real contact areas are reduced, and fluid films suppress molecular interactions.

Our results show that, under lubricated conditions at room temperature, the viscoelastic friction model provides excellent agreement with experimental data when strain softening of the rubber is properly taken into account. This softening, which reflects the reduction in effective modulus at large strain amplitudes, significantly enhances the predicted friction and must be considered in quantitative modeling. At lower temperatures ($T = -20°C$ and $-40°C$), the measured friction exceeds the theoretical predictions. We attribute this to partial penetration of the lubricant film by surface asperities, leading to increased solid-solid contact and greater energy dissipation due to adhesive contributions.

✉ B. N. J. Persson
b.persson@fz-juelich.de

1 State Key Laboratory of Solid Lubrication, Lanzhou Institute of Chemical Physics, Chinese Academy of Sciences, Lanzhou 730000, China

2 Peter Grünberg Institute (PGI-1), Forschungszentrum Jülich, 52425 Jülich, Germany

3 Multiscale Consulting, Wolfshovener str. 2, 52428 Jülich, Germany

4 Shandong Linglong Tire Co., Ltd, Zhaoyuan 265400, China

For dry surfaces, adhesion contributes significantly to the total friction force. By subtracting the viscoelastic component obtained under lubricated conditions, we estimate the adhesive shear stress in the real contact area. This shear stress increases approximately linearly with the logarithm of the sliding speed, consistent with thermally activated stick–slip mechanisms proposed in earlier studies.

Overall, our study demonstrates the importance of including both viscoelastic strain softening and contact mechanics in modeling sliding friction on rubber, and shows how experimental observations across different temperatures and surface conditions can be consistently interpreted within this framework.

2 Viscoelastic Modulus

In this study, we use the same carbon-filled styrene-butadiene rubber (SBR) compound as in the wear study in Ref. [4]. The viscoelastic modulus has been obtained using Dynamic Mechanic Analyzer (DMA) measurements in elongation mode for a strain amplitude of 4×10^{-4} (or 0.04% strain) [5]. At this small strain, we probe the linear response properties of the rubber. Fig. 1 shows (a) the real part ReE and the imaginary part ImE, and (b) the ratio $\mathrm{Im}E/\mathrm{Re}E = \tan\delta$ of the viscoelastic modulus as a function of frequency.

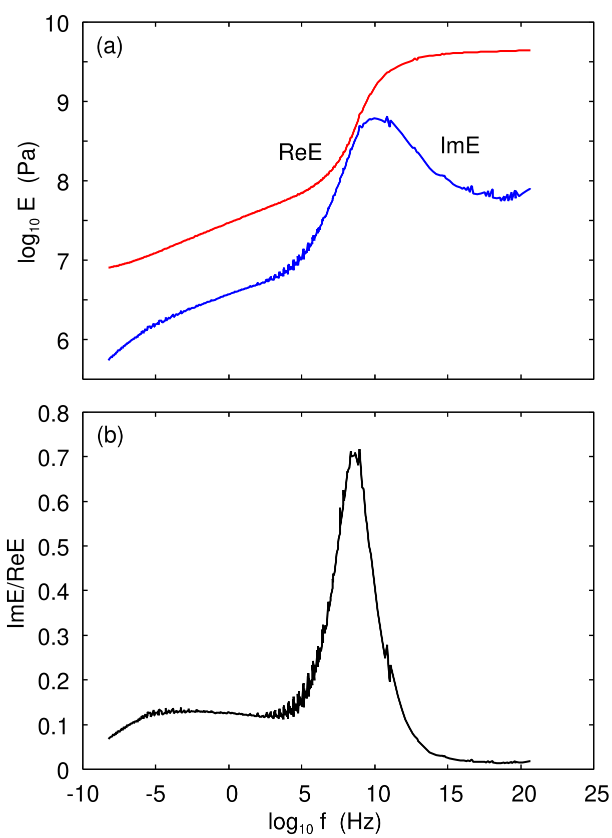

Fig. 1 **a** The real ReE and imaginary ImE part of the linear response viscoelastic modulus, and **b** the tan delta $\mathrm{Im}E/\mathrm{Re}E$ as a function of the frequency for the carbon filled SBR compound for $T = 20°\mathrm{C}$. The glass transition temperature of the rubber is $T_g = -50°\mathrm{C}$

We define the glass transition temperature T_g as the temperature T at which $\tan\delta(T)$, for the frequency $\omega_0 = 0.01\ \mathrm{s}^{-1}$, reaches its maximum. We found that using this definition yields a T_g that is nearly the same as that obtained using standard methods such as viscosity or calorimetry. For the SBR compound used in this study, this gives a glass transition temperature of $T_g \approx -50°\mathrm{C}$.

Rubber sliding (or rolling) friction typically involves relatively large strains and depends on the nonlinear viscoelastic properties of the rubber [6–8]. In this paper, we studied the large-strain dependence of the effective modulus. The measurements were performed at a frequency of $f = 1$ Hz and a temperature of $T = 20°\mathrm{C}$ in elongation mode. Fig. 2 shows the ratio $\eta_\mathrm{R}(\epsilon) = \mathrm{Re}E(\epsilon)/\mathrm{Re}E(0)$ (lower curve) and $\eta_\mathrm{I}(\epsilon) = \mathrm{Im}E(\epsilon)/\mathrm{Im}E(0)$ (upper curve) for the effective modulus at strain ϵ and at zero strain (actually $\approx 10^{-4}$), as a function of ϵ. For the strain values studied here $\eta_\mathrm{R}(\epsilon)$ decreases monotonically with increasing strain but for large ϵ is increases, and for very large ϵ, where the chain molecules are fully stretched, $\eta_\mathrm{R}(\epsilon)$ increases very fast with ϵ.

For the sliding wedge the strain below the wedge is complex with shear, elongation and compression deformations occurring in different spatial regions (see Appendix A). However, strain softening resulting from the breakdown of the filler network occurs in all types of deformation, as discussed in detail in Appendix B, where we also describe how the viscoelastic modulus was constructed.

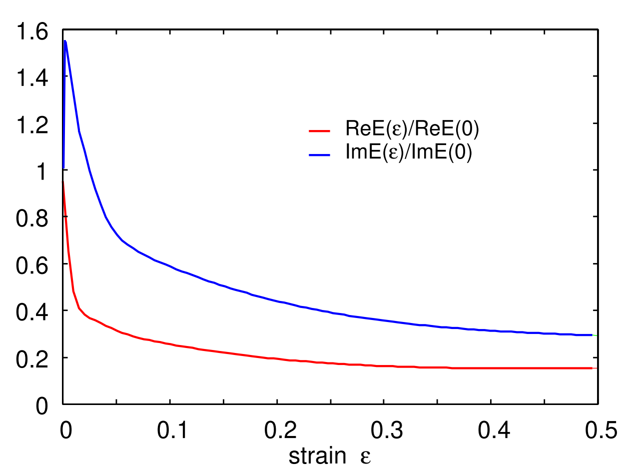

Fig. 2 The viscoelastic modulus at the strain ϵ divided by the modulus for the strain $\epsilon = 10^{-4}$ obtained for the frequency 1 Hz and the temperature $T = 20°\mathrm{C}$

3 Theory of Viscoelastic Contribution to Rubber Sliding Friction

We consider lubricated friction at low sliding speed and assume that the frictional shear stress in the area of real contact is negligible. The experimental results will be compared to the theory developed in Ref. [3] for rolling friction, which is also valid for lubricated sliding friction at low speed if the frictional shear stress is negligible.

The theory presented in Ref. [3] predicts the rolling friction for rigid spheres and cylinders on flat surfaces of viscoelastic solids. It was found to agree very well with the exact result of Hunter for rolling cylinders, for the simple rheological model used by Hunter [9]. Here, we apply the same theory to triangular steel profiles sliding on a lubricated rubber plate.

In this study, we use the triangular steel profiles shown in Fig. 3. A profile of length L_y is pressed against a flat rubber sheet (thickness d) with the normal force per unit length $f_N = F_N/L_y$, and slides at speed v. We first consider the symmetric wedge and later the asymmetric one. If the width $2a$ (in the sliding direction) of the footprint of the triangle and the rubber sheet satisfy $2a \ll d$, we can treat the rubber slab as infinitely thick. In this case, the sliding friction force [3] is given by

$$F_f = \frac{2(2\pi)^2}{v} \int d^2q \, \frac{\omega}{q} \mathrm{Im}\left[\frac{1}{E_{\rm eff}(\omega,\epsilon)}\right] |p(\mathbf{q})|^2, \tag{1}$$

where $q = |\mathbf{q}|$ and where $E_{\rm eff}$ is the effective viscoelastic modulus defined as $\mathrm{Re}E_{\rm eff}(\omega,\epsilon) = \eta_R(\epsilon)\mathrm{Re}E^*(\omega)$ and $\mathrm{Im}E_{\rm eff}(\omega,\epsilon) = \eta_I(\epsilon)\mathrm{Im}E^*(\omega)$, with $E^*(\omega) = E(\omega)/(1-\nu^2)$. Here, ϵ is the typical strain in the contact region (see below). The integration variable q represents the wavenumber and $\omega = \mathbf{q}\cdot\mathbf{v}$. In (1), $p(\mathbf{q})$ is the Fourier transform of the contact pressure $p(\mathbf{x})$.

We consider a symmetric triangular indenter with a half-opening angle α (see Fig. 4) pressed against an elastic half-space with a force per unit length $f_N = F_N/L_y$. The pressure distribution [10] is given by

$$p(x) = p_0 \cosh^{-1}\left(\frac{a}{x}\right) \tag{2}$$

To determine the prefactor p_0, we note that

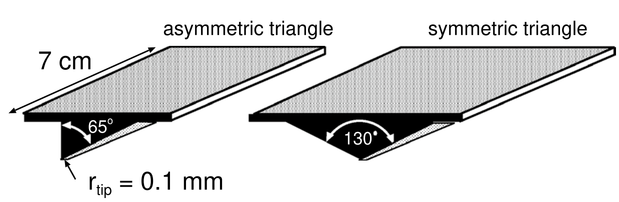

Fig. 3 The two triangular steel sliders used in the rubber friction experiments

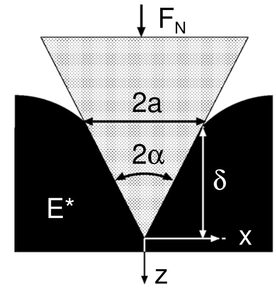

Fig. 4 The penetration is given by $\delta = a/\tan\alpha$. The length of the triangular indenter in the y-direction is L_y. The typical strain is approximately $\delta/a = \cot\alpha$

$$f_N = \int_{-a}^{a} dx \, p_0 \cosh^{-1}\left(\frac{a}{x}\right) = a p_0 \int_{-1}^{1} d\xi \, \cosh^{-1}\left(\frac{1}{\xi}\right)$$

Since $\cosh^{-1}$ is even and defined on $[1,\infty)$, we can write the integral as

$$f_N = 2ap_0 \int_0^1 d\xi \, \cosh^{-1}\left(\frac{1}{\xi}\right) = \pi a p_0$$

thus,

$$p_0 = \frac{f_N}{\pi a}$$

The half-width of the contact is

$$a = \frac{f_N}{E^* \cot\alpha}, \tag{3}$$

where $E^* = E/(1-\nu^2)$. When used in (1), E^* is replaced with $|E_{\rm eff}(\omega,\epsilon)|$, with $\omega = \mathbf{q}\cdot\mathbf{v}$, so the contact width $w = 2a$ depends on the sliding speed v. Fig. 5 shows the pressure $p(x)$ as a function of x for the symmetric indenter squeezed against the rubber with a normal force per unit length $F_N/L_y = 3000$ N/m. We use the effective elastic modulus corresponding to a contact time of the order of ~ 1000 s. The pressure distribution exhibits a (weak) singularity $p \sim \log|x|$ as $x \to 0$.

The average pressure is given by

$$\bar{p} = \frac{1}{2a}\int_{-a}^{a} dx \, p(x) = \frac{\pi}{2} p_0$$

or $\bar{p} = f_N/2a$. The penetration δ is given by (see Fig. 4):

$$\delta = \frac{a}{\tan\alpha}$$

The Fourier transform of the pressure is

$$p(\mathbf{q}) = \frac{1}{(2\pi)^2}\int d^2x \, p(\mathbf{x}) e^{-i\mathbf{q}\cdot\mathbf{x}} = \delta(q_y) p(q_x),$$

where

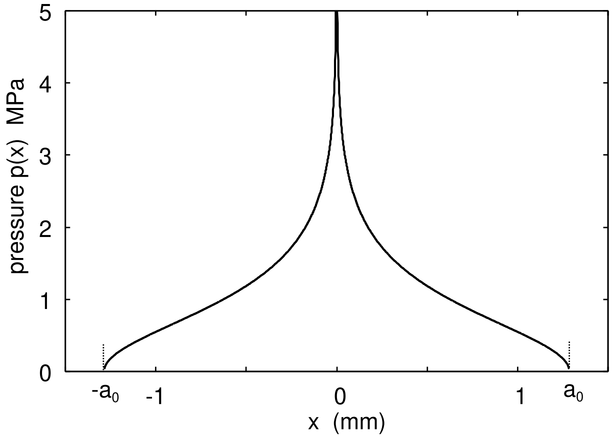

Fig. 5 The pressure $p(x)$ as a function of x for the symmetric indenter pressed against the rubber with a normal force per unit length $f_\mathrm{N} = 3000$ N/m. The effective elastic modulus, including a strain softening factor of 0.2, is taken as $E_\mathrm{eff}(1/t_0, \epsilon) = 25 \times 0.2 = 5$ MPa, corresponding to a contact time of approximately $t_0 \approx 1000$ s. The indenter tip is assumed to be perfectly sharp, $r_\mathrm{tip} = 0$. The width of the contact region is $w = 2a_0 \approx 2.5$ mm

$$p(q_x) = \frac{1}{2\pi} \int dx\, p(x) e^{-iq_x x}$$

$$= \frac{p_0}{2\pi} \int_{-a}^{a} dx \cosh^{-1}\left(\frac{a}{x}\right) e^{-iq_x x}$$

$$= \frac{p_0 a}{2\pi} \int_{-1}^{1} d\xi \cosh^{-1}\left(\frac{1}{\xi}\right) e^{-iq_x a\xi}$$

Define

$$g(q_x a) = \frac{1}{2\pi} \int_{-1}^{1} d\xi \cosh^{-1}\left(\frac{1}{\xi}\right) e^{-iq_x a\xi}$$

$$= \frac{1}{\pi} \int_{0}^{1} d\xi \cosh^{-1}\left(\frac{1}{\xi}\right) \cos(q_x a\xi)$$

we obtain

$$p(q_x) = \frac{f_\mathrm{N}}{\pi} g(q_x a) \tag{4}$$

Using

$$[\delta(q_y)]^2 = \delta(q_y) \cdot \frac{1}{2\pi} \int dy\, e^{-iq_y y} = \frac{L_y}{2\pi} \delta(q_y)$$

we get from (1):

$$\mu = \frac{F_\mathrm{f}}{f_\mathrm{N} L_y} = \frac{8\pi}{f_\mathrm{N}} \int_0^\infty dq_x \,\mathrm{Im}\left[\frac{1}{E_\mathrm{eff}(q_x v, \epsilon)}\right] |p_0(q_x)|^2$$

Substituting (4) gives:

$$\mu = \frac{8 f_\mathrm{N}}{\pi} \int_0^\infty dq_x \,\mathrm{Im}\left[\frac{1}{E_\mathrm{eff}(q_x v, \epsilon)}\right] |g(q_x a)|^2 \tag{5}$$

The triangular steel profiles have a finite tip radius of curvature $r_\mathrm{tip} = 0.1$ mm. We account for this by using a high-wavenumber cutoff in the integral (5), limiting $0 < q_x < q_1$ with $q_1 = 2\pi / r_\mathrm{tip}$.

The strain in the region where the viscoelastic deformations occur varies spatially, but is typically of the order

$$\epsilon = \frac{1}{2}\left(\frac{\partial u_z}{\partial x} + \frac{\partial u_x}{\partial z}\right) \approx \frac{1}{2}\frac{\partial u_z}{\partial x} \approx \frac{\delta}{2a} \approx \frac{1}{2\tan\alpha}. \tag{6}$$

As the sliding speed increases (or the temperature decreases), the effective modulus $E_\mathrm{eff}(qv, \epsilon)$ increases and the half-width a decreases, while the strain ϵ remains unchanged. In our case, $\epsilon \approx 0.23$. In the analysis below, we present theoretical results that include strain softening. These were obtained using the effective modulus $E_\mathrm{eff}(\omega, \epsilon)$ for the strain ϵ given by (6). This approach is, of course, approximate, since it is based on linear viscoelastic theory with a correction for nonlinearity introduced via an effective modulus that depends on the average strain in the contact region, while the actual strain varies in space. Still, comparison with experimental data (see below) shows that this approach provides a good estimation of the influence of strain softening on sliding friction.

For the strain $\epsilon \approx 0.23$, based on Fig. 2, we obtain $\eta_\mathrm{R} \approx 0.2$ and $\eta_\mathrm{I} \approx 0.4$. Since sliding friction depends on $\mathrm{Im}[1/E_\mathrm{eff}]$, the nonlinear (strain softening) correction will be significant, enhancing the sliding friction by roughly a factor of 5 (see below), which is similar to what was found in earlier rolling friction studies.

4 Experimental Results and Comparison to Theory

We used the same linear friction tester as in previous studies on sliding and rolling friction [11]. Two different triangular steel profiles (see Fig. 3) were attached to the force cell. The steel surfaces exhibit self-affine fractal roughness with a Hurst exponent $H \approx 0.77$, a roll-off wavenumber $q_\mathrm{r} \approx 2 \times 10^4$ m^{-1}, and a root-mean-square roughness $h_\mathrm{rms} = 1.5$ μm. A SBR plate of thickness 15 mm was fixed to the machine table, which was driven by a servo motor through a gearbox to produce translational motion. The relative velocity between the steel triangle and the rubber substrate was controlled, while the force cell recorded both the normal force and the friction force. The normal load per unit length was $F_\mathrm{N}/L_y = 3000$ N/m, and the sliding speed was varied from 1 μm/s to 1 cm/s. Both triangular steel sliders were 7 cm long in the y-direction, orthogonal to the sliding direction. The tip angles were 65° and 130°, and the tips have a radius of curvature $r_{tip} = 0.1$ mm.

In Fig. 6, we show two pressure footprints of the contact between the symmetric triangle slider and the rubber substrate obtained using a pressure-sensitive film. The metal triangle was loaded against the rubber surface with the film in between. The two footprints correspond to contact times of 6 s and 600 s, with widths (indicated by the blue bars) of 2 and 2.5 mm, respectively.

Fig. 7 shows the measured sliding friction for the symmetric triangle on dry (blue squares) and lubricated (green squares) rubber. The lubricated surface was prepared by spreading a teaspoon of silicone oil (DuPont Liveo 360 medical fluid, viscosity 0.97 Pa · s) over the rubber surface area (14 cm × 14 cm). Due to the low sliding speed and high contact pressure, the silicone oil acts as a boundary lubricant (without hydrodynamic effects) and likely eliminates or reduces any opening-crack contribution to the sliding friction (see below).

In Fig. 8, we compare the measured friction for the lubricated surface with the theoretical prediction at room temperature. The green squares are the experimental data from Fig. 7, and the red line is the theoretical prediction of the viscoelastic contribution to friction for the symmetric triangle. The theory involves no fitting parameters, and the agreement between theory and experiment is remarkably good. This

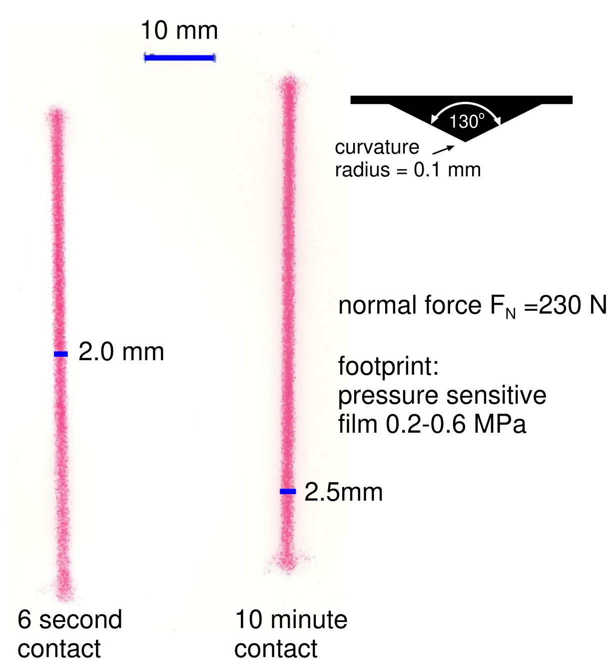

Fig. 6 The metal triangle loaded against the rubber surface with a pressure-sensitive film in between. The two footprints correspond to contact times of 6 s and 600 s, respectively. The two short blue bars indicate widths of 2 and 2.5 mm

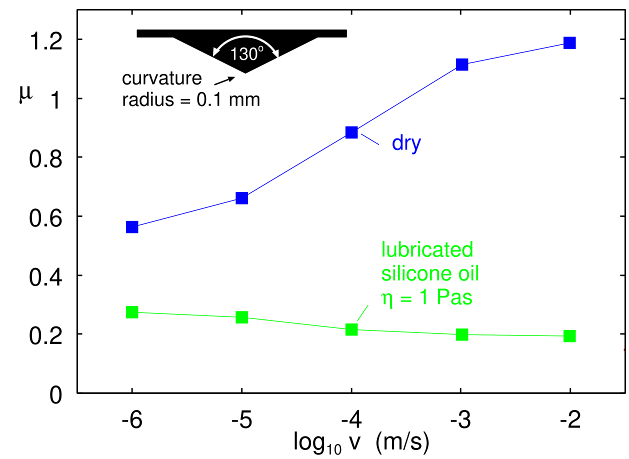

Fig. 7 Sliding friction for the symmetric triangle on dry (blue squares) and lubricated (green squares) rubber

result shows that, for the lubricated surface at $T = 20°$C, the measured friction is almost entirely due to the viscoelastic deformation of the substrate. This implies that the difference between dry and lubricated friction in Fig. 7 must result from the adhesive contribution in the area of real contact.

The red curve in Fig. 8 corresponds to the actual tip radius of 0.1 mm. The pink and blue curves represent theoretical results for $r_{tip} = 0.2$ and 0.05 mm, respectively. As expected, a sharper tip leads to slightly higher sliding friction, but the effect is small due to the weak (logarithmic) singularity of the contact pressure near the tip at $x = 0$ as $r_{tip} \to 0$.

Fig. 9 shows the dependence of the friction coefficient on the normal load for a symmetric slider sliding on a lubricated rubber substrate. The sliding velocity was $v = 3$ mm/s. The

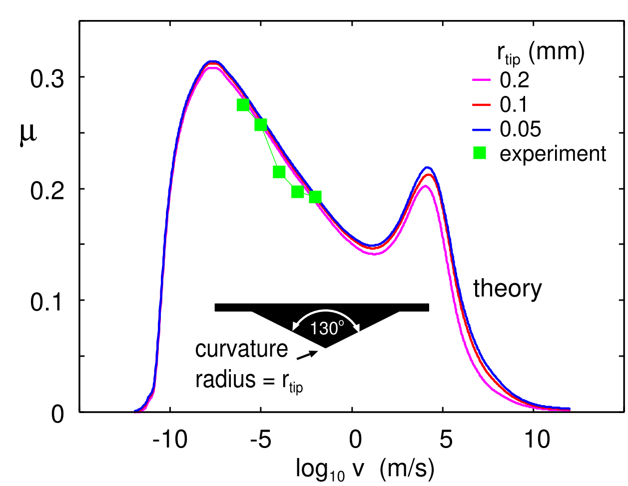

Fig. 8 Sliding friction for the symmetric triangle on the lubricated rubber surface (green squares from Fig. 7). The red line is the theoretically predicted viscoelastic contribution to the friction, assuming the measured tip radius $r = 0.1$ mm. The pink and blue lines show the predicted values for tip radii of 0.2 and 0.05 mm, respectively

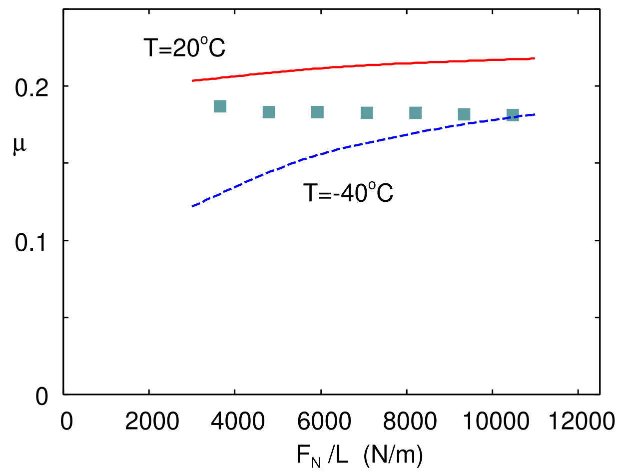

Fig. 9 Dependence of the friction coefficient on the normal load for a symmetric slider sliding on a lubricated rubber substrate. The measured data (squares) and the red line represent the experimental and theoretical results at $T = 20°C$. The blue dashed line corresponds to the calculated result at $T = -40°C$. Theoretical predictions of the viscoelastic contributions were obtained using the measured tip radius of $r = 0.1$ mm

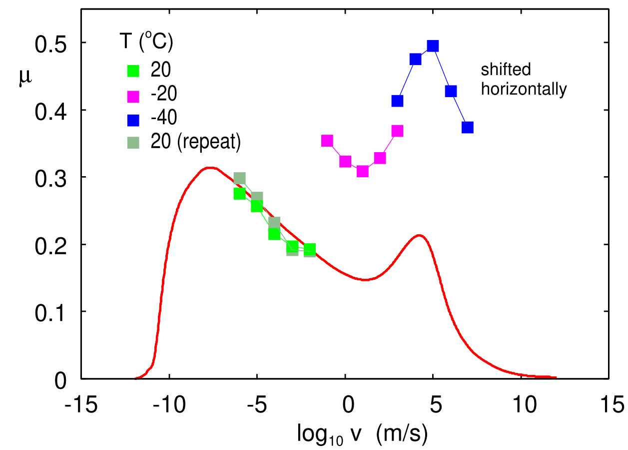

Fig. 10 Sliding friction for the symmetric triangle on lubricated rubber at $T = 20$ (green), -20 (pink), and $-40°C$ (blue), along with a repeated measurement at 20°C (dark green). The measured data for $-20°C$ and $-40°C$ are shifted horizontally using the viscoelastic bulk shift factor. The red line is the theoretically predicted viscoelastic contribution assuming a tip radius of $r = 0.1$ mm

measured data (squares) and the red line represent the experimental and theoretical results, respectively, at $T = 20°C$. The blue dashed line corresponds to the calculated result at $T = -40°C$. Theoretical predictions of the viscoelastic contributions were obtained using the measured tip radius of $r = 0.1$ mm. It can be seen that the friction coefficient in the theoretical prediction increases slightly with increasing load, whereas the experimental results exhibit the opposite trend and show a slight decrease in the friction coefficient with increasing load.

Fig. 10 shows the measured sliding friction for the symmetric slider on the lubricated rubber substrate at different temperatures: $T = 20°C$ (green data points, from Fig. 8), $-20°C$ (pink), $-40°C$ (blue), and a repeat measurement at 20°C (dark green). The red line represents the theoretically predicted viscoelastic contribution to the friction for the symmetric slider, based on the measured tip radius $r = 0.1$ mm. The measured data at $-20°C$ and $-40°C$ are shifted horizontally using the viscoelastic bulk shift factor, so that they correspond to the equivalent friction values at 20°C but at higher sliding speeds. However, these measured friction values lie significantly above the theoretical prediction (red curve).

We attribute the enhanced friction at $-20°C$ and $-40°C$ to the high contact pressure resulting from the increased elastic modulus of rubber at low temperatures, which may lead to penetration of the lubricant film by surface asperities. To support this interpretation, Fig. 11 shows the calculated width of the contact region as a function of sliding speed for $T = 20°C$, $-20°C$, and $-40°C$. The contact width is much smaller at the two lower temperatures, which corresponds to a higher contact pressure.

Nevertheless, the sliding friction at $-20°C$ and $-40°C$ remains lower than expected for dry surfaces, indicating that the lubricant film continues to reduce friction even under these colder conditions.

Assuming, as supported by the theory, that the sliding friction on the lubricated surface at room temperature is dominated by viscoelastic effects, we can estimate the shear stress acting in the area of real contact under dry conditions using

$$\tau_f(v) = [\mu(v) - \mu_{visc}(v)] \frac{F_N}{w(v)L_y}$$

Here, $\mu(v)$ is the total friction coefficient, and μ_{visc} is the viscoelastic contribution, as given by the green and blue curves in Fig. 7. The normal force is $F_N \approx 210$ N, and the real contact area is $A = wL_y$, where $w(v)$ is the width of the contact and $L_y = 7$ cm is the slider length. Note that $\tau_f(v)$ increases nearly linearly with the logarithm of the sliding speed, as expected for thermally activated processes in the low-velocity regime (See Fig.12).

If the interface is assumed to be very clean, meaning free from contamination films, the shear stress τ_f may originate from molecular stick–slip processes, as first suggested by Schallamach [12] and later studied in more detail by Persson and Volokitin [13]. However, Klüppel [14] and Carbone et al. [15] (see also [16–19]) have proposed that the adhesive contribution to sliding and rolling friction arises from the propagation of opening and closing cracks at the edges of the contact regions during sliding. This mechanism may be an

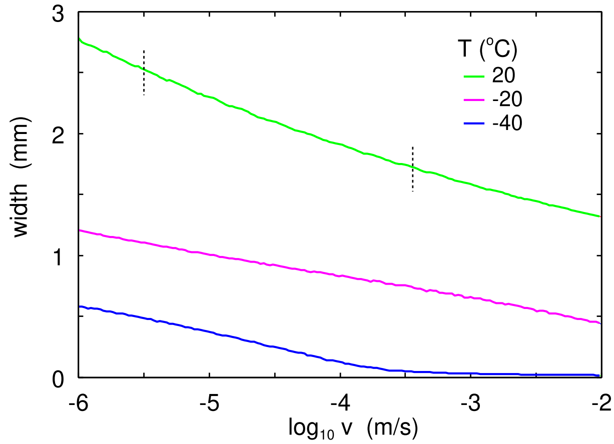

Fig. 11 The calculated contact width as a function of sliding speed, for temperatures $T = 20°C$, $-20°C$, and $-40°C$

important additional contribution for very soft rubber compounds with smooth surfaces sliding on relatively smooth substrates. For relatively stiff rubber compounds, such as those used in rubber seals or tires, and for most real surfaces used in practical applications, experimental evidence shows that the crack-opening mechanism contributes negligibly to sliding or rolling friction in most cases [1, 20]. This is primarily due to surface roughness, which suppresses or greatly reduces adhesion [21].

Fig. 11 shows the calculated width of the contact region as a function of the sliding speed. Note that at room temperature (green curve), the predicted widths are very similar

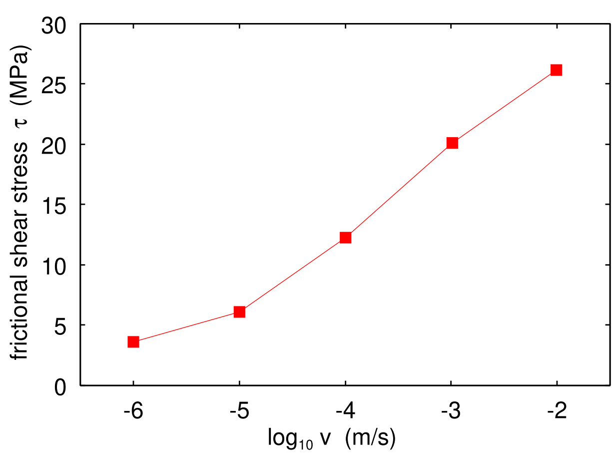

Fig. 12 The frictional shear stress in the area of real contact, obtained by subtracting the viscoelastic contribution $\mu_{visc}(v)$ from the total friction coefficient $\mu(v)$ (green and blue curves in Fig. 7), and multiplying the difference by the normal force $F_N \approx 210$ N. The result is divided by the contact area $A = w(v)L_y$, where $w(v)$ is the contact width and $L_y = 7$ cm: $\tau(v) = [\mu(v) - \mu_{visc}(v)]F_N/w(v)L_y$

to the contact width of 2–2.5 mm obtained using pressure-sensitive film (see Fig. 6). In fact, the results in Fig. 11 can be used to accurately estimate the contact width after 6 s and 600 s of stationary contact as follows.

During a time interval t, the slider moves a distance $d = vt$, so the contact width $d = 2$ mm observed after $t = 6$ s corresponds to a sliding speed of $v \approx d/t \approx 3 \times 10^{-4}$ m/s. Similarly, a contact width of $d = 2.5$ mm for $t = 600$ s corresponds to a sliding speed of $v = 4.2 \times 10^{-6}$ m/s. These two speeds are indicated by vertical dotted lines in Fig. 11, the corresponding contact widths are approximately $w \approx 1.8$ mm and 2.4 mm, respectively, in nearly perfect agreement with the measured footprint widths shown in Fig. 6.

It is important to note that this good agreement with the theory is obtained only when strain softening is included. Since the contact width $w = 2a$ is proportional to $1/E^*$ [see Eq. (3)], using the low-strain modulus would result in a predicted width approximately five times smaller than observed.

We have also performed sliding friction experiments for the asymmetric slider, but only under lubricated conditions. In this case, the friction differs significantly depending on the sliding direction. Fig. 13 shows that when sliding in the direction of the slope (forward), the friction is only slightly higher than that measured for the symmetric slider. When sliding in the direction of the vertical side of the steel sliders (backward), the friction is very high, approximately equal to 1, even on the lubricated surface. In this configuration, the edge of the steel profile likely penetrates the lubricant film, resulting in the high observed friction coefficient.

Fig. 14 shows the dependence of the friction coefficient on the normal load for the asymmetric slider sliding in the forward and backward directions on the lubricated rubber substrate. Notably, in the forward sliding direction, the friction coefficient increases slightly with increasing normal load. This trend contrasts with that observed for the

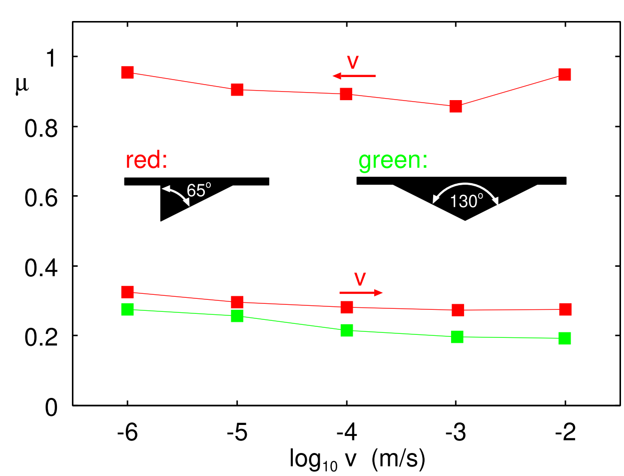

Fig. 13 Sliding friction for two triangular sliders on a lubricated rubber substrate

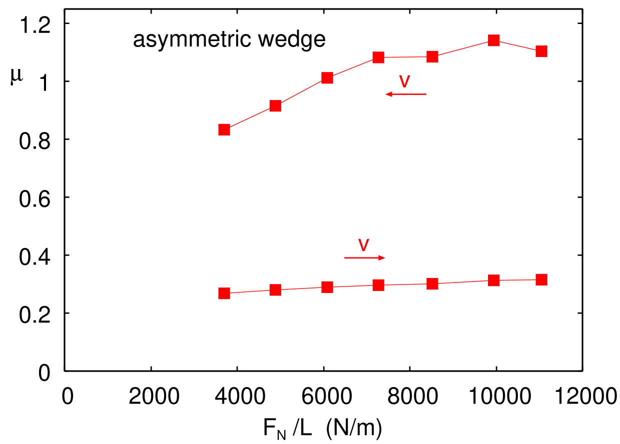

Fig. 14 Dependence of the friction coefficient on the normal load for an asymmetric slider sliding in the forward and backward directions on a lubricated rubber substrate

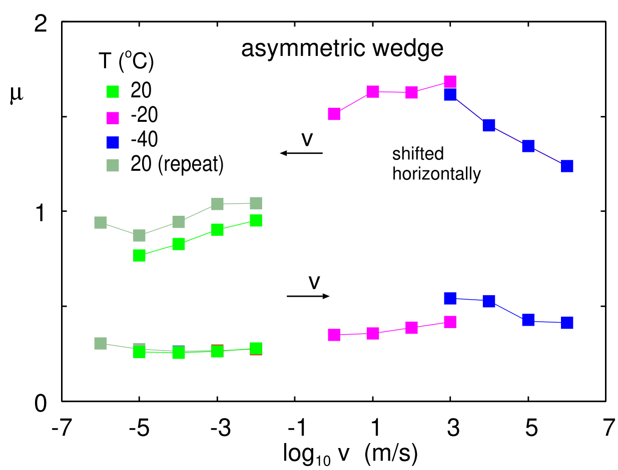

Fig. 15 Sliding friction for the asymmetric slider on the lubricated rubber at $T = 20°C$ (green), $-20°C$ (pink), and $-40°C$ (blue), along with a repeat measurement at 20°C (dark green). The measured data for $-20°C$ and $-40°C$ have been shifted horizontally using the bulk viscoelastic shift factor

symmetric slider, where the friction coefficient decreases slightly as the load increases, as shown in Fig. 9.

Fig. 15 presents the sliding friction for the asymmetric slider on the lubricated rubber at $T = 20°C$ (green), $-20°C$ (pink), and $-40°C$ (blue), along with a repeat measurement at 20°C (dark green). The data for $-20°C$ and $-40°C$ have been shifted horizontally using the bulk viscoelastic shift factor. At these lower temperatures, the measured friction in the forward sliding direction is comparable in magnitude to that of the symmetric slider.

For the asymmetric slider, we do not have numerical results for the viscoelastic contribution to friction. However, it is likely that, as in the case of the symmetric slider, the theoretical viscoelastic contribution is much smaller than the measured values. This discrepancy may result from penetration of the lubricant film at low temperatures, where the rubber is significantly stiffer than at room temperature and, as a result, the contact pressure is much higher.

5 Discussion

Greenwood and Tabor [1] found that the rolling friction coefficient for a steel sphere on a rubber surface was nearly the same as the sliding friction for the same sphere on the same rubber surface lubricated with a wet soap film. This indicates that, at least under the conditions of their study, the viscoelastic contribution dominates the friction.

They also studied the friction of cones on the same lubricated rubber surface and argued that, for large tip angles, the sliding friction is primarily viscoelastic. However, as the cone opening angle decreased, they observed a significant increase in friction, which they attributed to penetration of the lubricant film and tearing of the rubber. Specifically, cones with half-angles of 80°, 60°, and 50° produced practically no damage to the rubber and exhibited relatively low friction coefficients in the range of 0.1 to 0.2. In contrast, a 45° cone caused light wear, while a 30° cone produced substantial wear along the center of the contact region.

In our experiments, we observed no visible wear, even for the asymmetric slider moving on the unlubricated rubber surface in the direction of the vertical wall, where the friction coefficient was similarly high (on the order of 1) as that reported in Ref. [1] for the 30° cone. This difference may be due to the distinct wear properties of the rubber compounds used, although no information about the rubber type was provided in Ref. [1].

In a recent study, Ciavarella et al. [22] used the boundary element method to investigate the sliding friction of non-cylindrical punches with power-law profiles $|x|^n$ on a model "rubber" characterized by a single relaxation time. They observed good agreement with the prediction of Eq. (1) for $n = 2$ (case for Hunter [9]), but some deviations were found for larger values of n. However, they showed that if the solution for the cylindrical case ($n = 2$) was normalized using the modulus and mean pressure at zero sliding speed, a "universal" curve was obtained, which was valid for all studied exponents in the range $n = 2$ to 8.

Rubber filled with reinforcing particles exhibits strong strain softening. It is crucial in studies of rolling and sliding friction to account for the rapid decrease in effective modulus with increasing strain. This has been emphasized previously in the context of rolling friction [11], but it is equally important for sliding friction. In the present study, the strain in the contact region is approximately 0.23, which is similar to the strain encountered in asperity contacts when

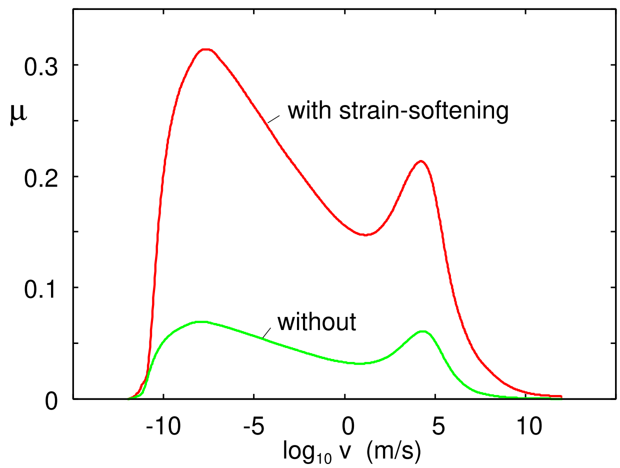

Fig. 16 Calculated sliding friction coefficient with strain softening (red line) and using the low-strain, linear response modulus (green curve), for the symmetric triangle assuming the measured tip radius $r = 0.1$ mm

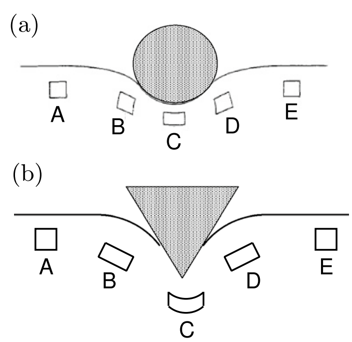

Fig. 17 The deformation of a rubber volume element as a **a** cylinder rolls on the rubber surface and **b** as a triangular wedge slides on a lubricated rubber surface. The result in **a** is adapted from Ref.[1]

a tire is in contact with a road surface. Fig. 16 compares the calculated friction using the linear response modulus $E(\omega)$ with the result obtained using the effective modulus defined by $\mathrm{Re}E_{\mathrm{eff}} = \eta_{\mathrm{R}}(\epsilon)\mathrm{Re}E(\omega)$ and $\mathrm{Im}E_{\mathrm{eff}} = \eta_{\mathrm{I}}(\epsilon)\mathrm{Im}E(\omega)$. The calculated result that includes strain softening yields friction that is approximately five times higher than the result without softening. A similarly strong effect of strain softening is observed in rolling friction and in sliding friction on rough surfaces such as road surfaces.

Appendix A: Deformation Field

Greenwood and Tabor [1] studied the strain when a cylinder is rolled over a block of rubber, and the distortion of grids painted on a lateral face of the rubber was photographed. The deformations of the rubber are shown in Fig. 17a. In the undisturbed part of the rubber is a square element A. As the ball rolls towards A, the element is first distorted to the (stretched and rotated) shape B, the greater part of the shear being parallel to the surface. When the element reaches the bottom of the ball, it is under compression. Between B and C there is a 45° rotation in the direction of shear. For the triangular wedge (Fig. 17b), we expect similar changes in the strain field, but the region of compressed rubber at the bottom of the wedge is reduced. The stress field below a blunted wedge was studied in Ref. [23], where they also studied frictional sliding, but assuming an elastic solid (no viscoelasticity).

Appendix B: Rubber Nonlinearity

All rubber compounds have nonlinear viscoelastic properties. We have assumed that the real and imaginary parts of the effective modulus can be written as $\mathrm{Re}E(\omega, T)\eta_{\mathrm{R}}(\epsilon)$ and $\mathrm{Im}E(\omega, T)\eta_{\mathrm{I}}(\epsilon)$, where $\eta_{\mathrm{R}}(\epsilon)$ and $\eta_{\mathrm{I}}(\epsilon)$ depend on the strain amplitude ϵ, and in principle also on frequency and temperature, but here we use $\eta(\epsilon)$ obtained at the frequency 1 Hz at the temperature $T = 20$°C. We note that the modulus obtained this way takes into account the nonlinearity using the secant method, which we believe is the best way to include nonlinearity in a linear response theory.

The viscoelastic master curve $E(\omega, T) = E(a_T\omega, T_0)$ and strain sweeps were performed in oscillatory tension mode using a Q800 DMA instrument produced by TA Instruments. We applied the oscillatory strain $\epsilon(t) = \epsilon_0 + \epsilon_1\cos(\omega t)$, where the pre-strain ϵ_0 was chosen to be $\epsilon_0 = 1.25\epsilon_1$ so that the rubber strip remained straight during the whole oscillation cycle. For the master curve, we used a very small strain amplitude, $\epsilon_0 = 0.0004$, and in this case, we are in the linear response region, where the modulus $E(\omega, T)$ is independent of the strain amplitude (and the pre-strain).

We note that the frequency-temperature shifting used to construct the master curve is strictly valid only when $E(\omega, T)$ is measured in the linear response region [5]. For the master curve, we measured $E(\omega, T)$ in frequency segments (between 0.1 and 100 Hz) and for temperatures between −80°C and 180°C. The frequency segments were shifted using the (unrestricted) procedure described in Ref. [5]. In Fig. 18, we show the shift factor a_T and also the WLF prediction using the canonical coefficients in the WLF expression. The WLF agrees with the result of the unrestricted shifting procedure only in a limited temperature interval.

The strain sweep used to construct $\eta_{\mathrm{R}}(\epsilon)$ and $\eta_{\mathrm{I}}(\epsilon)$ depends on the pre-strain. A better method would be to perform the strain sweeps in shear mode, but our DMA instrument cannot apply a large enough shear stress for such measurements for filled rubber compounds. Since the pre-strain contributes to the break-up of the filler network, and since the pre-strain increases in proportion to the dynamic strain amplitude, we

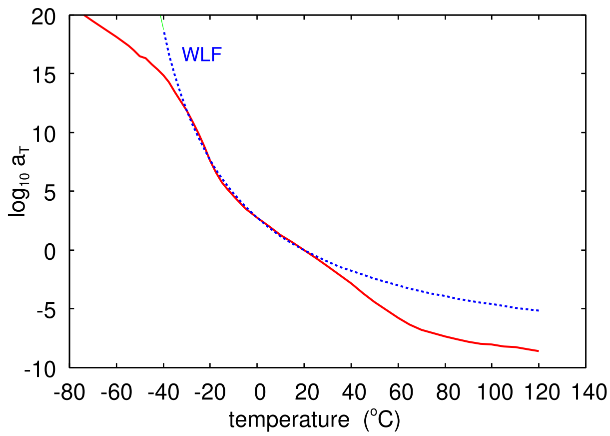

Fig. 18 The horizontal shift factor a_T as a function of temperature. The reference temperature is $T_0 = 20°\mathrm{C}$ and $a_{T_0} = 1$

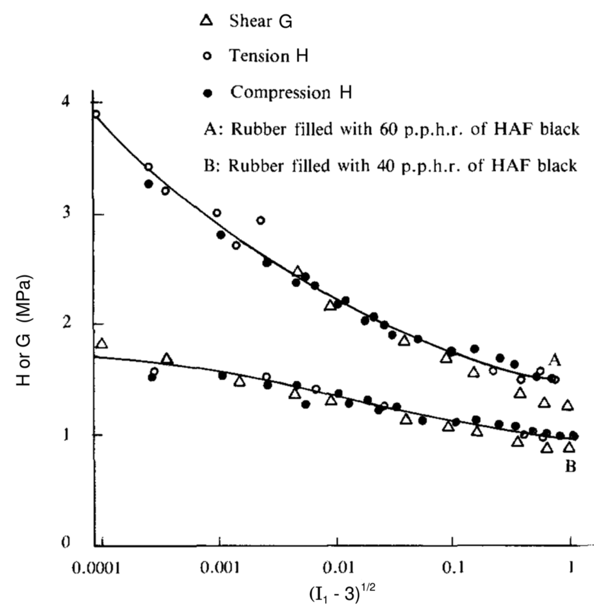

Fig. 19 Variation of H and G with strain invariant I_1, for natural rubber filled with 60 p.p.h.r. and 40 p.p.h.r. of HAF (N330) black. Adapted from [25, 26]

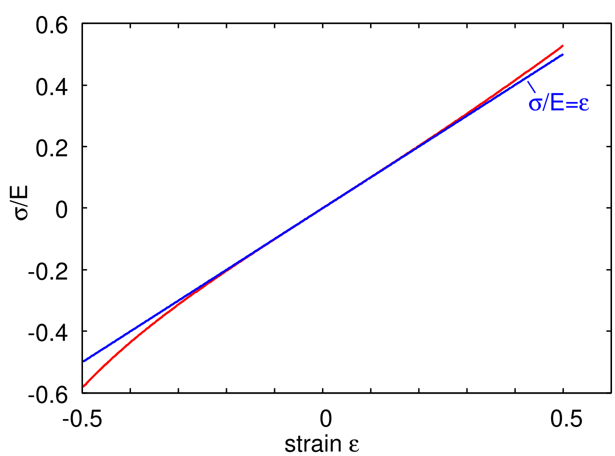

Fig. 20 Red curve: The dependency of the (physical) stress σ on the strain $\epsilon = \lambda_1 - 1$ [see (B3)]. Blue curve: The linear relation $\sigma/E = \epsilon$. The small-strain Young's modulus is denoted by E

expect faster strain softening with increasing strain amplitude for the strain sweep in tension compared to shear mode. However, we have shown in another study that using measurements in elongation and shear modes gives very similar results [24].

We have measured η_R and η_I using (oscillatory) elongation, but the strain field in the rubber below the wedge is more complex, with elongation, compression, and shear components (see Appendix A). Rubber with filler has a strongly nonlinear modulus for small strain (due, at least in part, to the breakdown of the filler network), but experimental studies have shown that this nonlinearity does not depend on the mode of deformation, at least in the static limit. Thus Gregory [25, 26] found that for a natural rubber compound with carbon black filler, the elastic energy stored in the deformed rubber can be accurately considered as a function of the strain invariant

$$I_1 = \lambda_1^2 + \lambda_2^2 + \lambda_3^2, \tag{B1}$$

where $\lambda_1 = L_x/L_0$ is the extension ratio in the x-direction and similarly for λ_2 and λ_3. Fig. 19 shows the effective modulus in elongation and compression, $H = \sigma/(\lambda - \lambda^2)$ ($H = E/3$ in the linear response region), and in shear, $G = \sigma/\gamma$, as a function of $(I_1 - 3)^{1/2}$. Clearly, the effective modulus is nearly independent of the mode of deformation up to $(I_1 - 3)^{1/2} \approx 1$. Physically, if the strain softening is due to the breakdown of the filler network as the rubber deforms, this should occur regardless of whether the sample is extended, compressed, or shear deformed. Hence, one expects strain softening to occur for small strain in all modes of deformation, as seen in Fig. 19. Assuming incompressible rubber so that $\lambda_1\lambda_2\lambda_3 = 1$, we have for elongation or compression in the x-direction, $\lambda_1 = L/L_0$ and $\lambda_2 = \lambda_3$, so that

$$I_1 = \lambda_1^2 + \frac{2}{\lambda_1}. \tag{B2}$$

Thus, $(I_1 - 3)^{1/2} = 1$ corresponds to $L/L_0 \approx 0.54$ (compression) or $L/L_0 \approx 1.68$ (elongation), so even larger strain than expected in our study.

The discussion above is for filled rubber. But even unfilled rubber exhibits an effective modulus that depends nonlinearly on the strain in elongation and compression. Here, we are interested in the physical stress σ, which is given by the force divided by the actual (strain-dependent) cross section. For the simple model where the elastic energy is proportional to I_1, one has [27]

$$\sigma = \frac{E}{3}\left(\lambda_1^2 - \frac{1}{\lambda}\right), \tag{B3}$$

where $\lambda = 1 + \epsilon$. We have plotted the relation between σ/E and ϵ in Fig. 20, and for the strain of interest in our applications, $\epsilon \approx 0.23$, we are, to a good approximation, in the linear region where the effective modulus is the same in extension as in compression and equal to E. For filled rubber compounds in the strain range $0 - 0.25$, most of the nonlinearity arises from the breakdown of the filler network, and not from the intrinsic nonlinearity arising from the dependency of the elastic energy on the strain invariants.

Acknowledgements We thank M. Ciavarella for the stimulating discussions that inspired this study. We thank Shandong Linglong Tire Co., Ltd, for support.

Author Contributions All authors contributed equally to the work. All authors read and approved the final manuscript.

Funding Open Access funding enabled and organized by Projekt DEAL. Not applicable.

Data Availibility The data are available from the corresponding author upon reasonable request.

Declarations

Competing interest The authors declare no competing interests.

Ethical Approval Not applicable.

Consent to Participate Not applicable.

Consent for Publication Not applicable.

References

1. Greenwood, J.A., Tabor, D.: The friction of hard slider on lubricated rubber: the importance of deformation losses. Proc. Phys. Soc. **71**, 989 (1958)
2. Sabey, B.E.: Pressure distributions beneath spherical and conical shapes pressed into a rubber plane, and their bearing on coefficients of friction under wet conditions. Proc. Phys. Soc. **71**, 979 (1958)
3. Persson, B.N.J.: Rolling friction for hard cylinder and sphere on viscoelastic solid. Eur. Phys. J. E **33**, 327 (2010)
4. Xu, R., Miyashita, N., Persson, B.N.J.: Rubber wear on concrete: dry and in-water conditions. Wear **578–579**, 206200 (2025)
5. Lorenz, B., Pyckhout-Hintzen, W., Persson, B.N.J.: Master curve of viscoelastic solid: using causality to determine the optimal shifting procedure, and to test the accuracy of measured data. Polymer **55**, 565 (2014)
6. Modeling of Non-Linear Viscoelastic Behavior of Filled Rubbers, Advances in Polymer Science 264 (2014) (Editor: Ponnamma, D., Thomas, S.)
7. Heinrich, G., Klüppel, M.: Recent advances in the theory of filler networking in elastomers. In: Lee, K.-S. (ed.) Advances in Polymer Science, vol. 160, pp. 1–44. Springer, Berlin (2002)
8. Tolpekina, T.V., Pyckhout-Hintzen, W., Persson, B.N.J.: Linear and nonlinear viscoelastic modulus of rubber. Lubricants **7**, 22 (2019)
9. Hunter, S.C.: The rolling contact of a rigid cylinder with a viscoelastic half space. J. Appl. Mech. **28**, 611 (1961)
10. Johnson, K.L.: Contact Mechanics. Cambridge University Press, Cambridge (1987)
11. Tiwari, A., Miyashita, N., Persson, B.N.J.: Rolling friction of elastomers: role of strain softening. Soft Matter **15**, 9233 (2019)
12. Schallamach, A.: A theory of dynamic rubber wear. Wear **6**, 375 (1963)
13. Persson, B.N.J., Volokitin, A.I.: Rubber friction on smooth surfaces. Eur. Phys. J. E **21**, 69 (2006)
14. Le Gal, A., Yang, X., Klüppel, M.: Evaluation of sliding friction and contact mechanics of elastomers based on dynamic-mechanical analysis. J. Chem. Phys. **123**, 014704 (2005)
15. Mandriota, C., Menga, N., Carbone, G.: Adhesive contact mechanics of viscoelastic materials. Int. J. Solids Struct. **290**, 112685 (2024)
16. Mastropasqua, M., Ronchi, A., Serra, A., Menga, N., Nicola., Carbone, G.: Adhesion and Friction in Viscoelastic Rough Contacts, Available at SSRN: https://ssrn.com/abstract=5272973 or https://doi.org/10.2139/ssrn.5272973
17. Nguyen, D.T., Paolino, P., Audry, M.C., Chateauminois, A., Fretigny, C., Chenadec, Y.L., Portigliatti, M., Barthel, E.: Surface pressure and shear stress fields within a frictional contact on rubber. J. Adhes. **87**, 235 (2011)
18. Müller, C., Müser, M.H., Carbone, G., Menga, N.: Significance of elastic coupling for stresses and leakage in frictional contacts. Phys. Rev. Lett. **131**, 156201 (2023)
19. Wei, H., Wang, Z., Tu, X., Cheng, X., Li, L., Wang, S., Li, C.: Does static friction information predict the onset of sliding for soft material? Int. J. Solids Struct. **305**, 113087 (2024)
20. Tiwari, A., Dorogin, L., Tahir, M., Stöckelhuber, K.W., Heinrich, G., Espallargas, N., Persson, B.N.J.: Rubber contact mechanics: adhesion, friction and leakage of seals. Soft Matter **13**, 9103 (2017)
21. Tiwari, A., Wang, J., Persson, B.N.J.: Adhesion paradox: why adhesion is usually not observed for macroscopic solids. Phys. Rev. E **102**, 042803 (2020)
22. Ciavarella, M., Tricarico, M., Papangelo, A.: Viscoelastic friction in sliding a non cylindrical asperity. Eur J Phys E **48**(4), 20 (2025)
23. Truman, C.E., Sackfield, A.: Closed-Form Solutions for the Stress Fields Induced by Blunt Wedge-Shaped Indenters in Elastic Half-Planes. J. Appl. Mech. **68**, 817 (2001)
24. Tolpekina, T.V., Pyckhout-Hintzen, W., Persson, B.N.J.: Linear and nonlinear viscoelastic modulus of rubber. Lubricants **7**(3), 22 (2019)
25. Othman, A.B., Gregory, M.J.: A stress-strain relationship for filled rubber. J. Nat. Rubb. Res. **5**, 144 (1990)

26. Gregory, M.J.: The Stress/Strain Behaviour of Filled Rubbers at Moderate Strains, Plast & Rubb: Mat. & Appl., November, p 18 (1979)
27. Gent A.N.: “Pneumatic Tire” . Mechanical Engineering Faculty Research. 854. http://ideaexchange.uakron.edu/mechanical_ideas/854 (2006)